Nuclear Engineering and Technology 56 (2024) 2239–2246

Contents lists available at ScienceDirect

Nuclear Engineering and Technology

journal homepage: www.elsevier.com/locate/net

Original Article

Radiological hazards assessment associated with granitoid rocks in Egypt

Ahmed E. Abdel Gawad [a], Masoud S. Masoud [a], Mayeen Uddin Khandaker [b,c], Mohamed Y. Hanfi [a,d,*]

[a] Nuclear Materials Authority, P.O. Box 530 El-Maadi, Cairo, Egypt
[b] Applied Physics and Radiation Technologies Group, CCDCU, School of Engineering and Technology, Sunway University, Bandar Sunway, 47500, Selangor, Malaysia
[c] Faculty of Graduate Studies, Daffodil International University, Daffodil Smart City, Birulia, Savar, Dhaka, 1216, Bangladesh
[d] Ural Federal University, St. Mira, 19, 620002, Ekaterinburg, Russia

ARTICLE INFO

Keywords:
Granitoid rocks
Building materials
Radioactive concentration
Hazards variables

ABSTRACT

The present study aimed to assess the radioactive hazards associated with the application of granitoid rocks in building materials. An HPGe spectrometer was used to detect the levels of the radioactive elements uranium-238, thorium-232, and potassium-40 in the granitoid rocks. The results showed that the levels of these elements were lower (38.32 < 33 Bq kg^{-1}), comparable (47.19–45 Bq kg-^{1}) and higher (992.26 ≫> 412 Bq kg^{-1}) than the worldwide limits for ^{238}U, ^{232}Th, and ^{40}K concentration, respectively. The exposure to gamma radiation of granitoid rocks was studied by various radiological hazard variables like the absorbed dose rate (D_{air}), the outdoor and indoor annual effective dose (AED_{out} and AED_{in}), and excess lifetime cancer risk (ELCR). A variety of statistical methods, including Pearson correlation, principal component analysis (PCA), and hierarchical cluster analysis (HCA) was used, to study the relationship between the radioactive elements and the radiological hazards. According to statistical analysis, the main radioactive risk of granitoid rocks is contributed to by the elements uranium-238, thorium-232, and potassium-40. Granitoid rocks can be applied in building materials, but under control to prevent risk to the public.

1. Introduction

Cities are under a lot of pressure from rapid population growth and infrastructure development. This can lead to chemical and radioactive contamination in different parts of the city [1,2]. Radiation in the environment comes from both natural and human-made sources [3]. Natural sources account for about 80 % of the radiation that people are exposed to each year [4,5]. Primordial radionuclides are the main natural sources of radiation in the environment. These are long-lived radionuclides that have been around since the Earth formed [6–8]. The most common primordial radionuclides are uranium-238, thorium-232, and potassium-40 [9–12]. The type of rock and soil in an area determines how these radionuclides are spread out [13,14]. Radionuclides can be transferred from rocks and soil to people in a variety of ways, such as by breathing them in, eating them, or touching them [15,16]. To better understand how much people are exposed to natural radiation, it is important to know the background radiation levels in an area [17,18]. The average activity concentrations in soil for uranium-238, thorium-232, and potassium-40 are 33, 45, and 412 Bq kg^{-1}, respectively. Gamma radiation from the ground has an exposure rate of about 59 nGy h^{-1} on average [19]. The background radiation on Earth is directly affected by the geological formation of the area. Cosmic rays and terrestrial radiation must also be considered when calculating the total exposure rate [20].

ATSDR's findings indicate that prolonged exposure to U, Ra, and their decay products can result in severe illnesses such as chronic lung disease, oral necrosis, leukopenia, or anaemia [21,22]. Furthermore, Th exposure can cause malignancies in the liver, kidneys [23], as well as bone, lung, and pancreatic cancer. Radionuclides are released and dissipated in the environment due to human activities, such as U mining [24,25]. Granitoids located in the area under study can be utilized for various infrastructure applications.

The Arabian-Nubian Shield (ANS) is composed of the basement complex of the Precambrian age along the two flanks of the Red Sea, located in northeastern Africa and western Arabia [26]. The ANS consists of a large orogenic belt which could be extended from Western Arabia to the East African Orogen (EAO) (Fig. 1a), through Saudi Arabia, Yemen, Oman, Jordan, Egypt, Sudan, Eritrea, Ethiopia and Somalia,

* Corresponding author. Ural Federal University, St. Mira, 19, 620002, Ekaterinburg, Russia.
E-mail address: mokhamed.khanfi@urfu.ru (M.Y. Hanfi).

https://doi.org/10.1016/j.net.2024.01.032
Received 19 December 2023; Received in revised form 16 January 2024; Accepted 23 January 2024
Available online 23 January 2024

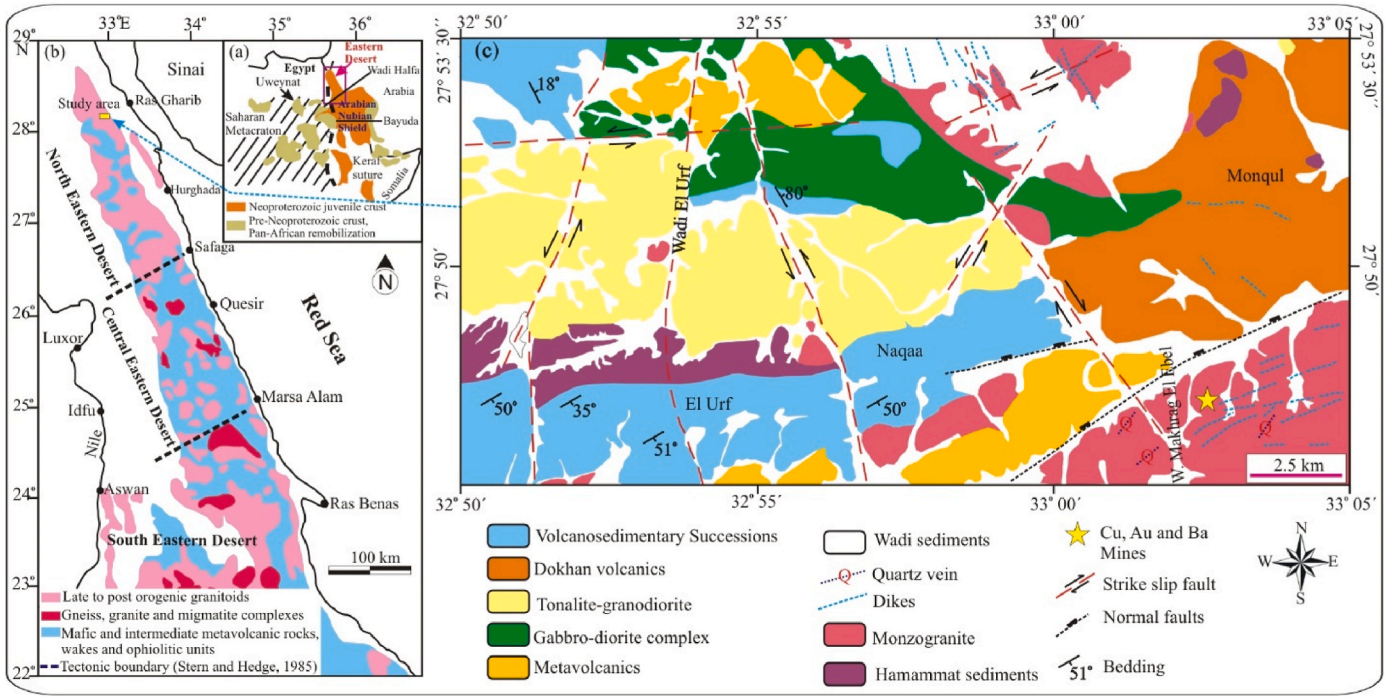

Fig. 1. (a) Geologic map shows the Arabian Nubian Sheild (ANS); (b) Geologic map shows the basement rocks of Neoproterozoic age in the (ED) of Egypt [26]; (c) Geologic map of El Urf–Monqul area, North Eastern Desert, Egypt.

whereas the southern belt occupies Mozambique segment.

The Eastern Desert (ED) is considered an important part of the ANS (Fig. 1b). Granitoid rocks are usefully utilized as decorative building materials, monuments, bridges, tile floors, and pavement sidewalks, due to their prestigious appearance and durability [27,28]. The building materials could be a good source of radiation exposure, particularly if they contain a higher proportion of natural and/or artificial radionuclides [29–31].

Based on the Agency for Toxic Substances and Disease Registry (ATSDR), exposure to U, Ra, and their decay products could cause serious illnesses, such as oral necrosis, chronic lung disease, anemia, and leukopenia [22,23] as well as kidney, liver, lung, bone, and pancreatic malignancies can all be induced by Th exposure [22]. The novelty of the present study is the assessment of the radiological hazards associated with the radionuclide's concentrations of the granitoid rocks.

2. Geological settings

The prospect area is covered mainly by the basement complex intruded by felsite and dolerite dikes as well as quartz and barite veins having N–S, NE–SW and E–W trends (Fig. 1c). The studied area is mainly traversed by many faults having N–S, NW–SE, NE–SW, and E–W trends.

Metavolcanics are considered the oldest rocks in the basement rocks of the El Urf – Monqul area. They occur in the southern and middle parts of the study area, and have been intruded by granitoids (tonalite-granodiorite and monzogranite). Metavolcanics form a thick sequence of stratified lava flows of dark green to gray meta-andesite, as well as metabasalt, metadacite, and metarhyolite to a lesser extent interbanded with their pyroclastics including ash tuffs, lapilli tuffs and lithic tuffs.

The gabbro-diorite complex is coarse-to medium-grained and occurs as elongated exposures in the central part of the prospect area. They were intruded on by the tonalite-granodiorite and monzogranite. They are hard, massive pale gray to dark green in color, and have exfoliation features. These rocks have low to medium relief and were intruded by tonalite-granodiorite and monzogranite.

The exposed older granitoid rocks (tonalite-granodiorite) form huge exposures in the central and northern parts of the Wadi El Urf area. They have low-to moderate-lying relief, medium-to coarse-grained, fractured, jointed, faulted, highly weathered, and vary from whitish gray to gray colors (Fig. 2a–c). These rocks are composed of plagioclase, quartz, K-feldspars, hornblende and biotite. They are affected by E–W, NE–SW and N–S fault trends.

Dokhan volcanic form huge exposure at Monqul area (Fig. 2d), and are massive, fine-grained, porphyritic and vary from black, dark green to gray, buff to reddish pink in colors. They have a thick sequence of lava flow and are mainly composed of basalt, andesite, rhyolite, rhyodacite and dacite interbedded with their pyroclastics such as ash tuffs, lapilli tuffs and lithic tuffs. They are composed mainly of andesite, basalt, rhyolite and dacite. Ignimbrite and imperial porphyry are well represented. The intercalations between Dokhan volcanic and Hammamat sediment form distinctive un-metamorphosed volcano-sedimentary successions in the southern part of the El Urf area [32–34].

The studied Dokhan volcanics are non-conformably overlain by a thick stratum of Hammamat sediments at El Urf – Monqul area in which the Hammamat sediments are composed of sandstone, siltstone, mudstones, and conglomerate (Fig. 2e). They are gray, grayish green, purple, red and brick in colors and were intruded by monzogranite.

The younger granite (monzogranite) crops out in the northern and southeastern parts of the Monqul area (Fig. 2d–f). Monzogranite plutons are massive, some exposure highly weathered and having onion-like bodies, vary from pink to pinkish red colors, and moderate relief. These rocks are medium-to coarse-grained and mainly composed of plagioclase, K-feldspar, quartz and biotite. The monzogranite in south Monqul is affected by intensive alterations bearing mineralization such as copper, barite and gold. Alterations are potassic, phyllic, argillic and prophylitic types. Copper minerals such astenorite, chrysocolla, chalcopyrite, enargite, bornite, and covellite are widely distributed at Wadi Makhrag El-Ebel of south Monqul [35–37].

3. Materials and methods

3.1. High purity germanium (HPGe) radiation detector

Following storage, the radionuclide activity concentration (A) of the

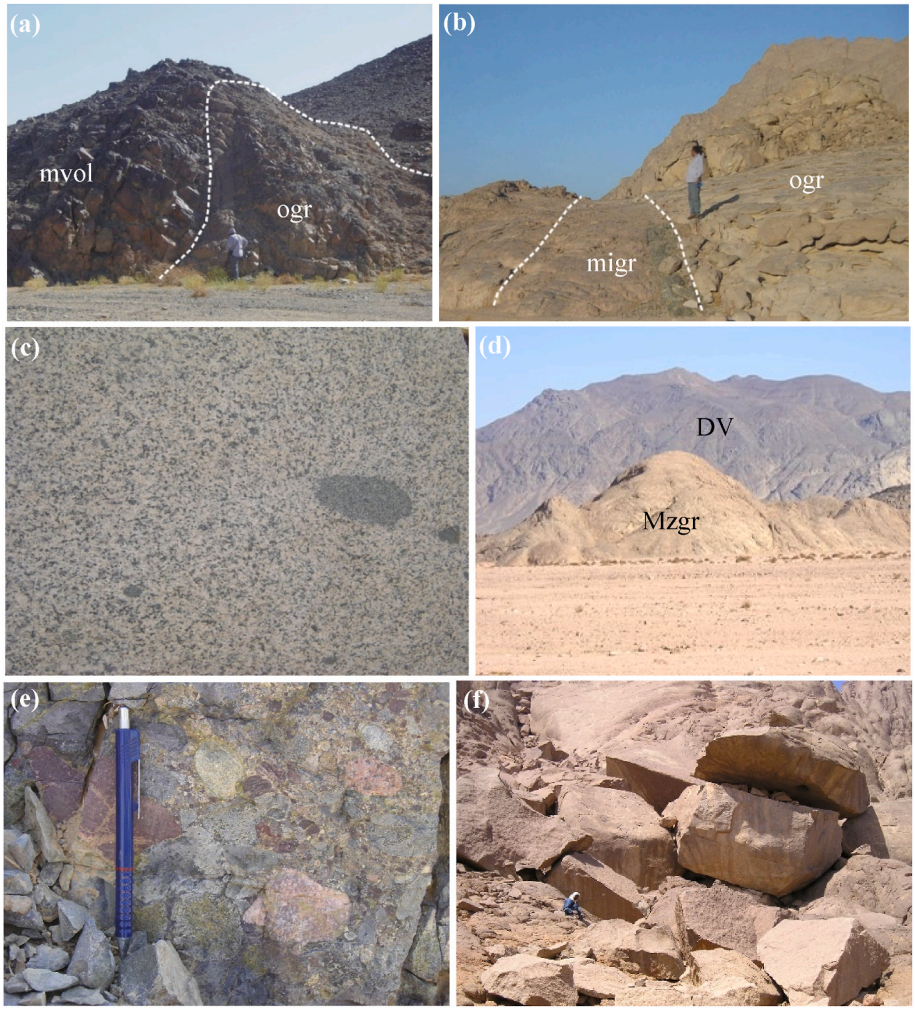

Fig. 2. (a) Older granitoid (ogr) (tonalite-granodiorite) intruded metavolcanic (mvol); (b) Microgranite dikes (migr) trending NNW–SSE invades older granitoid, (c) Close-up view showing oval-shaped xenolith of metavolcanic in older granitoid, (d) Monzogranites (Mzgr) intrude the Dokhan Volcanics (DV), (e) Close-up view of the Hamammat conglomerates, (f) Boulder appearance of monzogranites.

Granitoid Rocks samples is determined using a hyper pure germanium (HPGe) detector, model number GEM-15190 (high resolution of gamma radiation) at the Nuclear Material Authority of Egypt. Each sample took 70,000 s to analyze, which was done in a systematic manner. The resolution of the detector used—which was 1.85 keV for ^{226}Ra and 1332.5 keV for ^{60}Co—determines how much radioactivity may be detected in the sample. To demonstrate the energy calibration, the detectors have been calibrated using several sources of ^{241}Am, ^{226}Ra, and ^{60}Co before the test. These standard sources are certified by the USA as of 1994. Furthermore, the HPGe detector's efficiency curve was established in two stages throughout the energy spectrum from 186 to 2450 keV. The relative efficiency curve was originally detected in the first stage using the ^{226}Ra point source. After that, potassium chloride was used to normalize the HPGe mean relative curve [38]. An empty container that measured similarly and had the same geometry as the samples was used to identify the background before detection. To properly define the region of the identified isotopes' -spectrum, background spectra were used. The subsequent formula was used to figure out the concentrations of radionuclides (1).

$$A = \frac{N/t}{\varepsilon I_\gamma m} \tag{1}$$

where the radionuclide activity is denoted by A (Bq kg^{-1}), N is the total net count of the full-energy peak (peak areas are obtained by subtracting the background area from the total area), and t denotes the counting time (in seconds), I_γ, the γ - abundance, and the sample mass (m) are all referenced concerning the HPGe efficiency (ε) in the delivered γ -energy. The two naturally occurring ^{40}K radionuclides and the ray-producing nuclei in the disintegration of ^{238}U and ^{232}Th are the most significant natural radionuclides for this investigation. While ^{238}U and ^{232}Th are recognized indirectly for the gamma radiation emitters and their daughters, ^{40}K can be directly detected at 1460.7 keV. ^{226}Ra (186 keV), ^{214}Pb (352, 295 keV), ^{234}Pa (1001 keV), and ^{214}Bi (609, 1120, 1765 keV) are radionuclides that have been found, and their examination is what determines the amount of ^{238}U. While the activity concentration of ^{232}Th was calculated from the decay products in its series, ^{228}Ac and ^{208}Tl were measured from (911, 338.4 keV) and (583, 2614 keV), respectively. In addition, the photopeak (1460 keV) revealed a particular activity of ^{40}K [39]. The radionuclide-specific efficiency approach was used to calibrate the gamma spectrometry system's efficiency in order to keep out any uncertainty in gamma-ray intensities as well as the influence of coincidence summation and self-absorption effects of the producing gamma photons. Certified reference materials with densities comparable to the construction materials after pulverization, such as RGU-1, RGTh-1, and RGK-1, are used [40]. Based on the presumption that the radioactivity in the measurement samples is evenly distributed, the container geometry was selected. The minimum detection limits (MDL) for ^{238}U, ^{232}Th, and ^{40}K are calculated for each sample and divided by weight. Sample (M) calculation based on (MDL = (2.7 + 4.65

Table 1
Used radiological hazard indexes for the granitoid rocks, El Urf–Monqul area, Egypt.

Parameter	Definition	Formula
Absorbed dose rate D_{air} *(nGy h^{-1})*	dose rate exposure in the air at 1 m from radiation sources due to the concentrations (A) of^{238}U,^{232}Th and^{40}K	$D_{air} = 0.462\ A_U + 0.604\ A_{Th} + 0.0417\ A_K$
Outdoor annual effective dose AED_{in} *(mSv y^{-1})*	monitor the radiation exposure indoors and outdoors during a stationary period (1 y)	$AED_{out} = D_{air}$ (nGy h^{-1}) × 0.2 × 8760 (h y^{-1}) × 0.7 (Sv Gy^{-1}) × 10^{-6} (mSv. nGy^{-1})
Indoor annual effective dose AED_{out} (mSv y^{-1})		$AED_{in} = D_{air}$ (nGy h^{-1}) × 0.8 × 8760 (h/y) × 0.7 (Sv Gy^{-1}) × 10^{-6} (mSv nGy^{-1})
Excess Lifetime Cancer Risk - *ELCR*	probability of developing cancer over a lifetime at a given exposure level	$ELCR = (AED_{in} + AED_{out})$ × 70 y × 0.05

(B)1/2)/(MeIγt) [41], where B is the count of the background below the peak of interest, ε is the absolute value Efficiency, Iγ is the intensity of the gamma rays and t is counted. Time (seconds). For the elements ^{238}U, ^{232}Th, and ^{40}K, the minimum detectable activity (MDA) values are 2, 4, and 12 Bq kg^{-1}, respectively. The entire uncertainty of radiation levels was computed using regular and stochastic measurement errors. The radioactivity readings contain random errors of up to 5 %, while the efficiency calibration has regular inaccuracies of 0.5–2 % [42]. Table 1 shows the commonly used radiological hazard indexes estimated in the present study [43].

4. Results and discussion

4.1. Petrographic studies of granitoid rocks

Older granitoid rocks (tonalite-granodiorite) are medium-to coarse-grained, mesocratic with a grayish color and develop an equigranular hypidiomorphic texture. Microscopically, they consist of plagioclase, quartz, hornblende, biotite and K-feldspar. Accessory minerals are apatite, fluorapatite, titanite and iron-oxides, while secondary minerals include sericite, chlorite and epidote. Plagioclase is found as euhedral to subhedral crystals of oligoclase to andesine (An_{35-40}), showing lamellar twinning and mostly altered to sericite (Fig. 3a). Quartz occurs as large anhedral crystals with corroded outlines against plagioclase, hornblende and biotite and sometimes contains inclusions of sericitized plagioclase with fresh crystals of plagioclase (Fig. 3b). Hornblende is the main mafic mineral, usually present in larger amounts than biotite. It occurs as deep green color subhedral crystals, strongly pleochroic, consisting of two sets of cleavage (Fig. 3c) and some hornblende crystals show simple twinning (Fig. 3d) and are generally altered to biotite and chlorite (pennite) (Fig. 3e). Apatite is relatively the most abundant accessory mineral in the rock. It occurs as short prisms and needles enclosed in hornblende crystals (Fig. 3f). Fluorapatite occurs as a pale green crystal enclosed in quartz crystals (Fig. 3f). Titanite occurs as an accessory mineral in plagioclase and biotite. Opaque minerals form anhedral crystals associated with hornblende and biotite. Chlorite and epidote occur as alteration products of hornblende, biotite and plagioclase.

Monzogranite rocks are medium-to-coarse-grained, composed of plagioclase, k-feldspar, quartz and biotite. Apatite, allanite, zircon and opaque minerals are accessory minerals, while chlorite, epidote, muscovite and sericite are secondary minerals. Plagioclase occurs as euhedral to subhedral prismatic crystals characterized by lamellar twinning and partially to completely sericitized. K-feldspars occur as subhedral to anhedral crystals of microcline perthite showing cross-hatching and microperthite. Perthite enclosing plagioclase showing rapakivi texture (Fig. 3g and h). Quartz occurs as irregular anhedral crystals with corroded plagioclase and biotite. Biotite occurs as subhedral to euhedral crystals and is strongly pleochroic from brown to dark brown colors. Some crystals of biotite enclose plagioclase, zircon and opaque minerals (Fig. 3i and j). Alteration to chlorite and epidote is recorded. Allanite crystals are found occurring as euhedral to subhedral tabular prismatic crystals, reddish brown, zoned intimately associated with biotite and zircon (Fig. 3k). Zircon is found as euhedral prismatic crystals included in quartz (Fig. 3l). Opaque minerals form anhedral crystals associated with quartz and biotite. Apatite occurs as short prisms and needles enclosed in biotite crystals. Chlorite, muscovite and epidote occur as alteration products of biotite and plagioclase respectively.

4.2. ^{238}U, 232Th, and ^{40}K activity concentrations

Table 2 provides measurements for 67 of the granitoid samples that were collected for ^{238}U, ^{232}Th and ^{40}K activity concentrations. The overview of radionuclide activity concentrations and radiological parameters in the study zone is shown in Table 2 as well. ^{228}Th and ^{228}Ra are in equilibrium, while the activity of ^{228}Ac and ^{232}Th are approximately equivalent. Therefore, in this document, ^{232}Th is taken to be ^{228}Th, and vice versa. The average activity levels of ^{238}U, ^{232}Th, and ^{40}K in granitoid samples are significantly lower than the globally authorized average activity statistics of 32, 45, and 412 Bq kg^{-1}, respectively [5]. Table 2 offers a summary of the radionuclides concentration data. The enrolled means and standard deviations (Min/Max) for the activity concentrations of ^{238}U, ^{232}Th, and ^{40}K Mean ± SD (Min/Max) are 38.32 ± 14.93 (4.94/67.93), 47.19 ± 12.32 (21.92/89.73) and 992.26 ± 272.49 (281.70/1596.30) Bq kg^{-1}, respectively. It illustrated that the mean concentrations of thorium and potassium are comparable and higher than the worldwide average, respectively according to the UNSCEAR recommendations [5]. Table 2 additionally displays the statistical description for the activity levels of the natural radionuclides ^{238}U, ^{232}Th, and ^{40}K in the granitoid samples, including mean, skewness, kurtosis, and coefficient of variation (CV).

The frequency of the distribution was assessed for each linked radionuclide (histograms are shown in Fig. 4(a-c)). The normal distribution was achieved at ^{238}U, ^{232}Th, and ^{40}K concentrations. The normal distribution for radioelement ^{238}U, ^{232}Th and ^{40}K is due to the complexity of radioactive minerals in the granitoid samples.

Furthermore, the resilience of thorium minerals to weathering led to higher concentrations in certain samples. Additionally, uranium is more susceptible to leaching than thiium, leading to faster occurrence of high levels [44]. The increase in radioelement concentration may be linked to the natural concentration of the area under study's current of the granitoid rocks in general and uranium, thorium and potassium minerals in particular. The skewness data identified an asymmetric distribution that was consistent with the basic statistical analysis of radioelement activity concentrations, with favorable results pointing to an asymmetric distribution. Even though they refer to their negative conclusions as negative data, the tail of the asymmetric distribution is expanded. As a result, the data on ^{232}Th activity concentrations' positive skewness suggest that the asymmetry is positive, but the data on ^{238}U and ^{40}K activity concentrations' negative skewness suggest that the asymmetry is negative. Second, the values of the kurtosis represent the Preakness of the distribution probability. The activity and normal distributions are asymmetrical, as shown by the radioactive materials ^{232}Th, which both have kurtosis coefficients above 1. In contrast, the kurtosis coefficient for samples ^{238}U and ^{40}K was less than 1, which indicates that the probability distribution is flat. The data in Table 2 show that the standard deviation is lower than the mean of all linked radionuclides, including ^{238}U, ^{232}Th, and ^{40}K, demonstrating the high degree of uniformity of the predicted radionuclides in the granitoid samples. It can be shown in Table 2, that the moderate CV values of 39 %, 29 % and 27 % for detected radionuclides ^{238}U, ^{232}Th, and ^{40}K respectively. The differences in radiation levels may be due to the presence of minerals that contain uranium, thorium and potassium in the samples that were

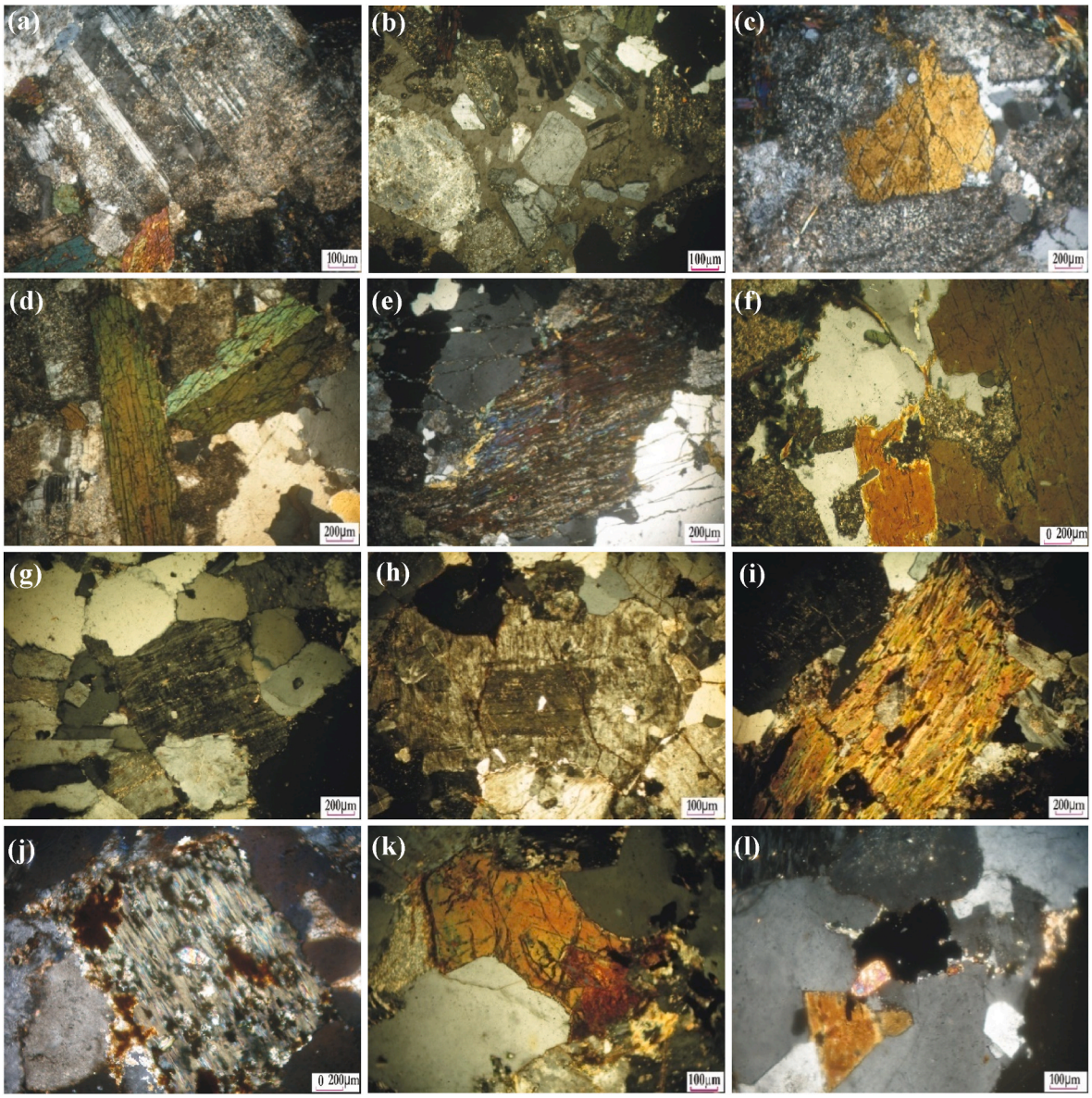

Fig. 3. Photomicrographs of the studied granitoids. (a) Plagioclase photomicrographs showing lamellar twinning and altered to sericite in older granitoid, (C.N.), (b) Quartz crystal enclose fresh and altered plagioclase feldspars in older granitoids (C.N.), (c) Hornblende showing two sets of cleavage surrounded by sericitized plagioclase in older granitoids, (C.N.), (d) Hornblende showing simple twinning in older granitoids, (C.N.), (e) Hornblende altered to kinked pennite in older granitoids (C.N.), (f) Quartz enclose pale green fluroapatite whereas hornblende enclose pale gray apatite (rode like) in older granitoids (C.N.), (g) Microcline perthite showing cross-hatching in monzogranite, (C.N.), (h) Plagioclase enclosed in perthite showing rapakivi texture in monzogranite, (C.N.), (i) Altered biotite crystal enclosing sericitized plagioclase with opaque minerals in monzogranite, (C.N.), (j) highly altered biotite into ferri-chlorite (pennite), and enclose zircon crystal in monzogranites, (C.N.), (k) Zonation of allanite crystals in monzogranite, (C.N.), (l) Quartz enclose zircon and opaque minerals in monzogranite, (C.N.). (For interpretation of the references to color in this figure legend, the reader is referred to the Web version of this article.)

Table 2
Descriptive statistics of data corresponding to the activity of radionuclides.

	N	Mean	SD	Min	Max	Skewness	Kurtosis	CV, %
^{238}U (Bq kg^{-1})	67	38.32	14.93	4.94	67.93	−0.20	−0.62	39
^{232}Th (Bq kg^{-1})	67	47.19	12.32	21.92	89.73	1.06	1.68	26
^{40}K (Bq kg^{-1})	67	992.26	272.49	281.70	1596.30	−0.18	0.08	27

studied.

It can be shown that 49 % of the granitoid samples had activity levels of ^{238}U that were higher than the mean value, 40 % of the samples had activity levels of ^{232}Th that were higher than the mean value, and 52 % of the samples had activity levels of ^{40}K that were higher than the mean value.

Table S1 lists the comparison of the most recent results of the activity concentrations of ^{238}U, ^{232}Th, and ^{40}K with the information from the prior review. This comparison demonstrates how the geological characteristics of any examined area mostly determine the radioactive activity concentrations. The current findings about the activity concentrations of ^{238}U, ^{232}Th, and ^{40}K show results that are either lower

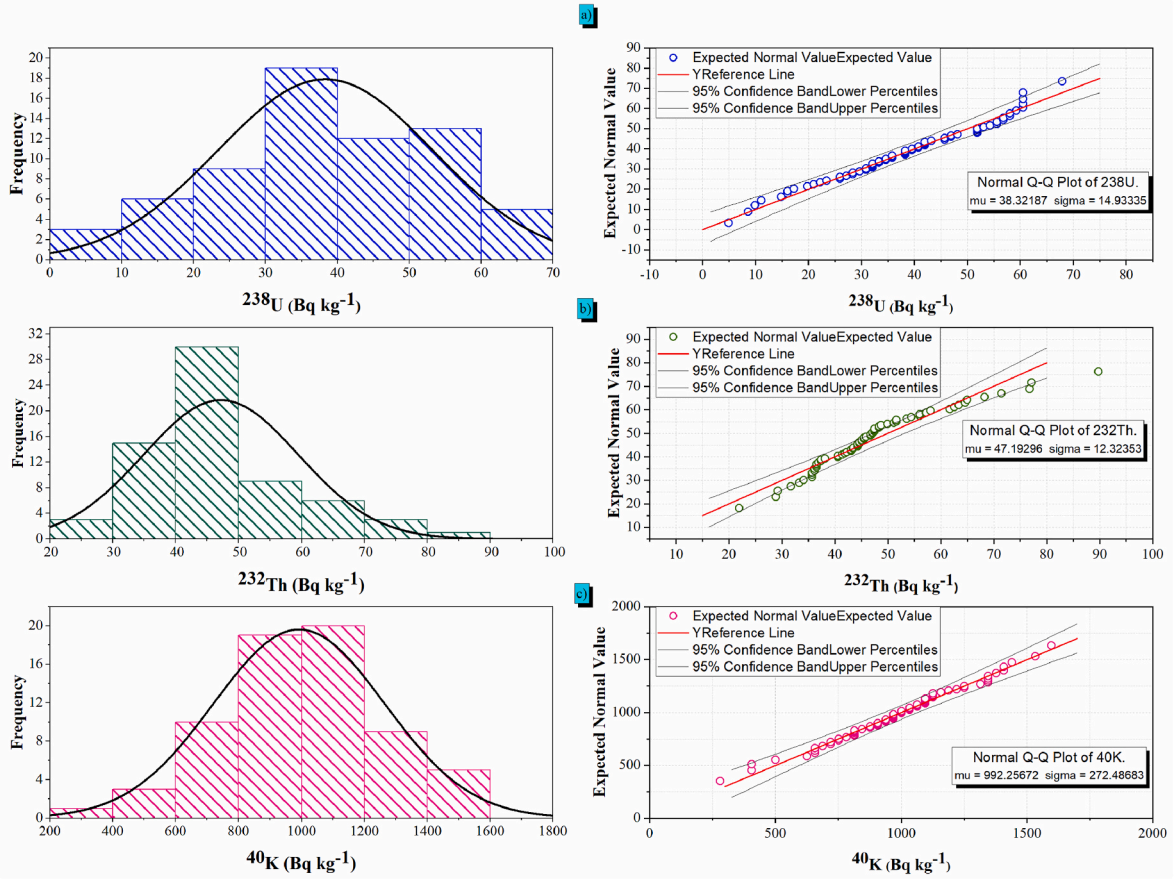

Fig. 4. Frequency distribution analysis and Q-Q plot of ^{238}U, ^{232}Th and ^{40}K in the granitoid samples at El-Urf area.

Table 3
Radiological hazard indexes in the 67 granitoid samples of the El Urf area.

	N	Average	Standard deviation	Minimum	Maximum
D_{air} (nGy h^{-1})	67	86.89	13.58	61.20	120.83
AED_{out} (mSv y^{-1})	67	0.11	0.02	0.08	0.15
AED_{in} (mSv y^{-1})	67	0.43	0.07	0.30	0.59
ELCR x 10^{-3}	67	1.86	0.29	1.31	2.59

or comparable to those from earlier studies.

4.3. Radiological hazard indices

The radiological hazard indexes determine the assessment of granitoid rocks from the El-Urf area of Egypt used as construction materials: Table 3 shows that the absorbed dose rate D_{air} varied between 61.20 and 120.83 nGy h^{-1}, with a mean value of 86.89 nGy h^{-1} that is higher than the UNSCEAR recommended amount of 58 nGy h^{-1} [5]. Consequently, the higher granitoid samples can be produced photons can damage humans, and long-term exposure to radioactive material will be safe. Indoor and outdoor annual effective dose AED_{in} and AED_{out} mean values are 0.11and 0.43 mSv y^{-1}, respectively, which are higher than the recommended averages of 0.07 mSv y^{-1} (outdoor) and 0.40 mSv y^{-1} (indoor) [5]. This means that long-term low-level exposure has adverse health repercussions such as tissue degeneration, DNA in genes, cancer, or cardiovascular disease [45]. The probability of developing cancer over a lifetime at a given exposure level is defined by the excess lifetime cancer risk (ELCR), is found the mean value of ELCR (1.86×10^{-3}) lower than the threshold limit 2.9×10^{-3} [46], where the range of ELCR values is varied from 1.31×10^{-3} to 2.59×10^{-3}.

Table 4
Results of normality tests.

Radionuclide	Kolmogorov-Smirnov*		
	DF	Statistic	Asymp. Sig. (2 tail)
^{238}U	67	0.09	0.69
^{232}Th	67	0.15	0.08
^{40}K	67	0.07	0.95

Asymp. sig. = asymptotic significance level. DF = degrees of freedom. * Lilliefors significance correction.

Table 5
The concentrations of radionuclides^{238}U,^{232}Th, and^{40}K and the radiological hazard indices.

	^{238}U	^{232}Th	^{40}K	D_{air}	AED_{out}	AED_{in}	ELCR
^{238}U	1	−0.06	−0.19	0.33	0.33	0.33	0.33
^{232}Th	\\	1	−0.05	0.47	0.47	0.47	0.47
^{40}K	\\	\\	1	0.70	0.70	0.70	0.70

4.4. Statistical analysis

Data analysis and histograms were analyzed using a multivariate statistical method that was developed using IBM SPSS version 21. 0, formerly known as IBM's commercial statistics software. A normal distribution was tested using the Kolmogorov–Smirnov (KS) test, as shown in Table 4. All tests showed a p-value greater than 1 %, supporting the null hypothesis that the natural radionuclide activity in beach sands is

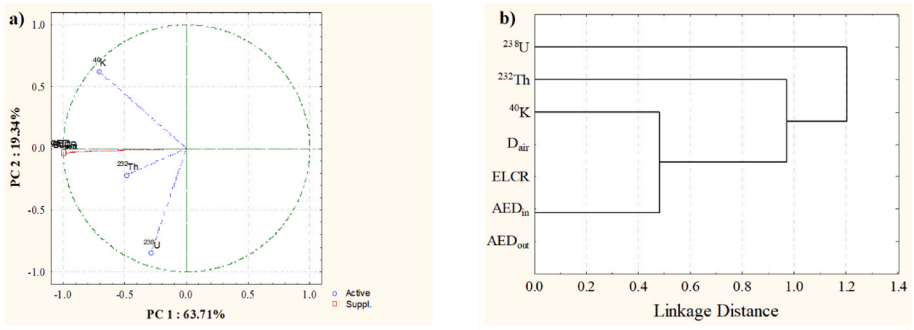

Fig. 5. Graphical representation of (a) PCA analysis and (b) dendrogram from hierarchical cluster analysis of radionuclides content and radiological hazard indexes in 67 samples of granitoid rocks.

normal.

Pearson correlation analysis was employed in the present study to establish the relationship between the radioactive elements (Table 5). The degree of association was classified into weak (0.00–0.19), moderate (0.2–0.39) strong (0.4–0.79) and very strong (0.8–1. 00) relationships [47]. A negative weak correlation between ^{238}U and ^{232}Th ($R^2 = 0. -0.06$) and also between ^{232}Th and ^{40}K (Table 5). A significant moderate positive correlation has been observed between the ^{238}U and the radiological hazard parameters, while a strong correlation with ^{232}Th and ^{40}K indicates their involvement in various natural radioactive decay pathways. The reason for this is the association of radiological variables with two radionuclides, which are recognized as the primary sources of gamma radiation in nature.

To further investigate the connection between 238U, 232Th and 40K activity concentrations and radiological hazard indicators, PCA is used to analyze 67 samples of granitoid rocks from the El-Urf in Egypt. Fig. 5a displays the components PC1 and PC2. They were identified. PC1 is heavily reliant on activity levels of 40K and radiological hazard indicators (63. 71 %). Naturally occurring radioactive deposits of 40K were found in the granitoid rocks at the work site. However, the PC2 load amounts to 19.34 % of 238U, and 232Th. The radiological hazard indices behavior is also indicative of this using multivariate algorithms, the hierarchical cluster analysis (HCA) is a data categorization method that differentiates various data types. This process involves measuring the Euclidean distance between radiological hazard indexes and radioactive activity concentrations. Fig. 5b presents a dendrogram of the investigated data, which is made up of three major clusters from the HCA output. Cluster I includes ^{238}U, cluster II comprises 232Th, and cluster III contains ^{40}K and radiological hazard indexes. The radioactive content of uranium and thorium is connected to the radioactivity of granitoid rocks, as suggested by HCA.

5. Conclusion

This study investigates how radioactive materials are distributed in granitoid rocks and how they might have gotten there. In the study several radiation hazard parameters, including the dose rate, the annual effective dose, and the excess lifetime cancer risk are estimated. They used multivariate statistical techniques such as Pearson correlation, principal component analysis, and hierarchical cluster analysis to study the relationship between radionuclides and their corresponding radiation hazard variables. The results of this study showed that the activity levels of uranium-238, thorium-232, and potassium-40 in granitoid rocks are 38.32 ± 14.93, 47.19 ± 12.32, and 992.26 ± 272.49 Bq kg-1, respectively. These levels are lower than the worldwide average for uranium (33 Bq kg-1) and comparable for thorium (45 Bq kg^{-1}) and higher approximately three times for potassium (412 Bq kg^{-1}). The radioactivity in granitoid rocks is mainly caused by the presence of uranium, thorium, and potassium. Building materials made from the most granitoid rocks are not likely to pose any danger to the public.

Data availability statement

All data generated or analyzed during this study are included in this published article.

Declaration of competing interest

The authors declare that they have no known competing financial interests or personal relationships that could have appeared to influence the work reported in this paper.

Appendix A. Supplementary data

Supplementary data to this article can be found online at https://doi.org/10.1016/j.net.2024.01.032.

References

[1] K.G. Taylor, P.N. Owens, Sediments in urban river basins: a review of sediment-contaminant dynamics in an environmental system conditioned by human activities, J. Soils Sediments 9 (2009) 281–303, https://doi.org/10.1007/s11368-009-0103-z.
[2] M.Y. Hanfi, I. V Yarmoshenko, A.A. Seleznev, M. V Zhukovsky, The gross beta activity of surface sediment in different urban landscape areas, J Radioanal Nucl Chem 321 (2019) 831–839. https://doi.org/10.1007/s10967-019-06657-9.
[3] R. Ravisankar, J. Chandramohan, A. Chandrasekaran, J. Prince Prakash Jebakumar, I. Vijayalakshmi, P. Vijayagopal, B. Venkatraman, Assessments of radioactivity concentration of natural radionuclides and radiological hazard indices in sediment samples from the East coast of Tamilnadu, India with statistical approach, Mar. Pollut. Bull. 97 (2015) 419–430, https://doi.org/10.1016/j.marpolbul.2015.05.058.
[4] M.Y. Hanfi, B.M. Emad, M.I. Sayyed, M.U. Khandaker, D.A. Bradley, Natural radioactivity in the prospecting tunnel in Egypt: dose rate and risk assessment, Radiat. Phys. Chem. 187 (2021) 109555, https://doi.org/10.1016/j.radphyschem.2021.109555.
[5] UNSCEAR, SOURCES and EFFECTS of IONIZING RADIATION United Nations Scientific Committee on the Effects of Atomic Radiation, 2010.
[6] A. El-Taher, F. Alshahri, R. Elsaman, Environmental impacts of heavy metals, rare earth elements and natural radionuclides in marine sediment from Ras Tanura, Saudi Arabia along the Arabian Gulf, Appl. Radiat. Isot. 132 (2018) 95–104, https://doi.org/10.1016/j.apradiso.2017.11.022.
[7] I. Gaafar, M. Hanfi, L.S. El-Ahll, I. Zeidan, Assessment of radiation hazards from phosphate rocks, Sibaiya area, central eastern desert, Egypt, Appl. Radiat. Isot. 173 (2021) 109734, https://doi.org/10.1016/j.apradiso.2021.109734.
[8] M.Y. Hanfi, Radiological assessment of gamma and radon dose rates at former uranium mining tunnels in Egypt, Environ. Earth Sci. 0 (2019), https://doi.org/10.1007/s12665-019-8089-3.
[9] P. Bala, R. Mehra, R.C. Ramola, Distribution of natural radioactivity in soil samples and radiological hazards in building material of Una, Himachal Pradesh, J. Geochem. Explor. 142 (2014) 11–15, https://doi.org/10.1016/j.gexplo.2014.02.010.
[10] P. Bangotra, R. Mehra, R. Jakhu, K. Kaur, P. Pandit, S. Kanse, Estimation of 222Rn exhalation rate and assessment of radiological risk from activity concentration of 226Ra, 232Th and 40K, J. Geochem. Explor. 184 (2018) 304–310, https://doi.org/10.1016/j.gexplo.2017.05.002.
[11] S. Forkapic, J. Vasin, I. Bikit, D. Mrdja, K. Bikit, S. Mili, Correlations between soil characteristics and radioactivity content of Vojvodina soil, J. Environ. Radioact. 166 (2017) 104–111, https://doi.org/10.1016/j.jenvrad.2016.04.003.

[12] T. Kovács, G. Szeiler, F. Fábián, R. Kardos, A. Gregorič, J. Vaupotič, Systematic survey of natural radioactivity of soil in Slovenia, J. Environ. Radioact. 122 (2013) 70–78, https://doi.org/10.1016/j.jenvrad.2013.02.007.
[13] R. Jakhu, R. Mehra, P. Bangotra, K. Kaur, H.M. Mittal, Estimation of terrestrial radionuclide concentration and effect of soil parameters on exhalation and emanation rate of radon, J. Geochem. Explor. 184 (2018) 296–303, https://doi.org/10.1016/j.gexplo.2017.03.002.
[14] F.C.A. Ribeiro, J.I.R. Silva, E.S.A. Lima, N.M.B. do Amaral Sobrinho, D.V. Perez, D. C. Lauria, Natural radioactivity in soils of the state of Rio de Janeiro (Brazil): radiological characterization and relationships to geological formation, soil types and soil properties, J. Environ. Radioact. 182 (2018) 34–43, https://doi.org/10.1016/j.jenvrad.2017.11.017.
[15] A. Dołhańczuk-Śródka, Estimation of external gamma radiation dose in the area of Bory Stobrawskie forests (PL), Environ. Monit. Assess. 184 (2012) 5773–5779, https://doi.org/10.1007/s10661-011-2380-4.
[16] S. DaPelo, M.M. Aghdam, V. Dentoni, A. Loi, P. Randaccio, Q. Crowley, Assessment of natural radioactivity and radon release potential of silurian black shales, Radiat. Phys. Chem. 215 (2024) 111347, https://doi.org/10.1016/j.radphyschem.2023.111347.
[17] A. Navas, L. Gaspar, M. López-Vicente, J. MacHín, Spatial distribution of natural and artificial radionuclides at the catchment scale (South Central Pyrenees), Radiat. Meas. 46 (2011) 261–269, https://doi.org/10.1016/j.radmeas.2010.11.008.
[18] L. Barbosa da Silva, L. Faria da Silva, C. Omar, P. Orejuela, V.B. Junior, A.X. da Silva, Assessment and estimation of the effective dose due to external exposure from natural radioactivity of sands used in civil construction in the state of Rio de Janeiro,Brazil, Appl. Radiat. Isot. 205 (2024) 111157, https://doi.org/10.1016/j.apradiso.2023.111157.
[19] UNSCEAR, Exposures from natural radiation sources (Annex B), Sources and Effects of Ionizing Radiation (2000) 84–141.
[20] A. Shahrokhi, M. Adelikhah, S. Chalupnik, T. Kovács, Multivariate statistical approach on the distribution of natural and anthropogenic radionuclides and associated radiation indices along the north-western coastline of Aegean Sea, Greece, Mar. Pollut. Bull. 163 (2021), https://doi.org/10.1016/j.marpolbul.2021.112009.
[21] ATSDR, Toxicological Profile for Uranium, Public Health Service, U.S. Department of Health and Human Services, 1999, pp. 1–145.
[22] ATSDR, Draft toxicological profile for radon: agency for toxic substances and disease registry 9–11 (2012) 161–167.
[23] ATSDR, Case Studies in Environmental Medicine, Public Health Service, U.S. Department of Health and Human Services, 1992, pp. 1–28.
[24] M.A. Hilal, M.F. Attallah, G.Y. Mohamed, M. Fayez-hassan, Evaluation of radiation hazard potential of TENORM waste from oil and natural gas production, J. Environ. Radioact. 136 (2014) 121–126, https://doi.org/10.1016/j.jenvrad.2014.05.016.
[25] Y.A. Abdel-Razek, M.S. Masoud, M.Y. Hanfi, M.S. El-Nagdy, Effective radiation doses from natural sources at Seila area South Eastern Desert, Egypt, Journal of Taibah University for Science 10 (2016) 271–280. https://doi.org/10.1016/j.jtusci.2015.06.010.
[26] J.P. Liégeois, R.J. Stern, Sr-Nd isotopes and geochemistry of granite-gneiss complexes from the Meatiq and Hafafit domes, Eastern Desert, Egypt: No evidence for pre-Neoproterozoic crust, J. Afr. Earth Sci. 57 (2010) 31–40.
[27] N.M. Moghazy, A.M. El-Tohamy, M.M. Fawzy, H.A. Awad, H.M.H. Zakaly, S.A. M. Issa, A. Ene, Natural radioactivity, radiological hazard and petrographical studies on Aswan granites used as building materials in Egypt, Appl. Sci. 11 (2021) 6471, https://doi.org/10.3390/app11146471, 2021.
[28] M.Y. Hanfi, A.E. Abdel Gawad, H. Eliwa, K. Ali, M.I. Sayyed, M.U. Khandaker, D. A. Bradley, Assessment of radioactivity in granitoids at Nikeiba, south Eastern Desert, Egypt; radionuclides concentrations and radiological hazard parameters, Radiat. Phys. Chem. (2022), https://doi.org/10.1016/j.radphyschem.2022.110113.
[29] A.E. Abdel Gawad, E.M. Ibrahim, Activity ratios as a tool for studying uranium mobility at El Sela shear zone, southeastern Desert, Egypt, J. Radioanal. Nucl. Chem. 308 (2016) 129–142.
[30] Y. Amin, M.U. Khandaker, A. Shyen, R. Mahat, R. Nor, D. Bradley, Radionuclide emissions from a coal-fired power plant, Appl. Radiat. Isot. 80 (2013) 109–116.
[31] M.Y.M. Hanfi, M.S. Masoud, M.I. Sayyed, M.U. Khandaker, M.R.I. Faruque, D. A. Bradley, M.Y.A. Mostafa, The presence of radioactive heavy minerals in prospecting trenches and concomitant occupational exposure, PLoS One 16 (2021) e0249329.
[32] C. Breitkreuz, H.A. Eliwa, I.M. Khalaf, Kh ElGameel, B. Bühler, S. Sergeev, A. Larionov, M. Murata, Neoproterozoic SHRIMP U–Pb zircon ages of silica-rich Dokhan volcanics in the North Eastern desert, Egypt, Precambrian Res. 182 (2010) 163–174.
[33] H.A. Eliwa, C. Breitkreuz, I. Khalaf, K. El Gameel, Depositional styles of early ediacaran terrestrial volcano-sedimentary succession in the gebel El Urf area, North Eastern desert, Egypt, J. Afr. Earth Sci. 57 (2010) 328–344.
[34] A.A. Abdel Wahed, K.G. Ali, M.M. Khalil, A.E. Abdel Gawad, Dokhan volcanics of gabal Monqul area, North Eastern desert, Egypt: geochemistry and petrogenesis, Arabian J. Geosci. 5 (2012) 29–44, https://doi.org/10.1007/s12517-010-0136-z.
[35] N.S. Botros, Genesis of gold mineralization in the North Eastern desert, Egypt, Ann. Geol. Surv. Egypt XX (1995) 381–409, 1994-1995.
[36] N.S. Botros, M.A. Wetait, A possible porphyry copper mineralization in South Monqul, Eastern Desert, Egypt, Egypt. J. Geol. 41–1 (1997) 175–196.
[37] A.E. Abdel Gawad, H. Eliwa, K.G. Ali, K. Alsafi, M. Murata, S.M. Masoud, M. Y. Hanfi, Cancer risk assessment and geochemical features of granitoids at nikeiba, southeastern desert, Egypt, Minerals 12 (2022) 621, https://doi.org/10.3390/min12050621.
[38] J.H. Al-Zahrani, Journal of Radiation Research and Applied Sciences Estimation of natural radioactivity in local and imported polished granite used as building materials in Saudi Arabia, J Radiat Res Appl Sci 10 (2017) 241–245, https://doi.org/10.1016/j.jrras.2017.05.001.
[39] B. Merdano, Radioactivity concentrations and dose assessment for soil samples from kestanbol granite area, Radiat. Protect. Dosim. 121 (2006) 399–405, https://doi.org/10.1093/rpd/ncl055.
[40] IAEA, Preparation and Certification of IAEA Gamma-Ray Spectrometry Reference Materials RGU-1, RGTh-1 and RGK-1, 1987. Iaea-Rl-148 48.
[41] A. Abbasi, Radiation risk assessment of coastal biota from a quasi-Fukushima hypothetical accident in the Mediterranean Sea, Mar. Pollut. Bull. 194 (2023) 115363, https://doi.org/10.1016/j.marpolbul.2023.115363.
[42] A. Papadopoulos, G. Christofides, A. Koroneos, L. Papadopoulou, C. Papastefanou, S. Stoulos, Natural radioactivity and radiation index of the major plutonic bodies in Greece, J. Environ. Radioact. 124 (2013) 227–238, https://doi.org/10.1016/j.jenvrad.2013.06.002.
[43] I.K. Ahmed, H.N.B. Khalaf, F. Ambrosino, et al., Fly ash radiological characterization from thermal power plants in Iraq, J. Radioanal. Nucl. Chem. 329 (2021) 1237–1245, https://doi.org/10.1007/s10967-021-07907-5.
[44] J.J. Heckman, R. Pinto, P.A. Savelyev, Natural elemental concentrations and fluxes: their use as indicators of repository safety, SKI Report 97 (2002) 29, 29 97.
[45] USEPA, EPA Radiogenic Cancer Risk Models and Projections for the, U.S. Population, 2011.
[46] A.A. Qureshi, S. Tariq, U. Kamal, S. Manzoor, C. Calligaris, A. Waheed, ScienceDirect Evaluation of excessive lifetime cancer risk due to natural radioactivity in the rivers sediments of Northern Pakistan, J Radiat Res Appl Sci 7 (2014) 438–447, https://doi.org/10.1016/j.jrras.2014.07.008.
[47] M.J. Abedin, M.R. Karim, M.U. Khandaker, M. Kamal, S. Hossain, M.H.A. Miah, D. A. Bradley, M.R.I. Faruque, M.I. Sayyed, Dispersion of radionuclides from coal-fired brick kilns and concomitant impact on human health and the environment, Radiat. Phys. Chem. 177 (2020) 109165, https://doi.org/10.1016/j.radphyschem.2020.109165.